FINE TUNING SCAFFOLDS FOR CULTIVATED MEAT PRODUCTION

Ayaan Shah

University College London

Department of Biochemical Engineering

INTRODUCTION

Traditional meat production places heavy pressure on land, water and climate: across around 38,000 farms studied globally, animal products consistently carry far higher greenhouse-gas emissions and land use than most plant-based foods, with beef and dairy dominating impacts[i].Beyond ecosystems, intensive livestock systems raise persistent animal-welfare concerns (confinement, stress, disease burden), which many scholars now treat as a core dimension of food-system sustainability[ii]. A further public-health risk is antimicrobial resistance (AMR): antimicrobial use in food animals is large and rising, increasing selective pressure for resistant bacteria that can move through food, environment, and direct contact pathways[iii]. Further research link livestock antimicrobial use with elevated resistance in zoonotic bacteria[iv].

Cultivated meat, muscle and fat tissue grown from animal cells using tissue-engineering methods, aims to decouple meat supply from livestock, potentially shrinking land occupation and greenhouse-gas emissions relative to conventional meat (noting that outcomes depend on future process design and energy sources)[v]. Realizing edible, structured muscle, however, is not a "cells-alone" problem: cells require a three-dimensional microenvironment that supports attachment, proliferation, alignment, and differentiation, and that ultimately yields meat-like texture. Hence, scaffolds are considered a central enabling technology for cultured meat[vi].

Hydrogel scaffolds made from food-compatible polysaccharides are attractive because they gel under mild, aqueous conditions and can be processed with cell-friendly chemistries. Alginate—an anionic copolymer from brown algae, ionically crosslinks with Ca^{2+} to form "egg-box" networks widely used for cell encapsulation; pectin, an anionic plant heteropolysaccharide, forms related Ca^{2+}-mediated networks and has shown biocompatibility in biomedical applications[vii]. Blending alginate with pectin can tune gelation kinetics, mechanics, and microstructure; prior work demonstrates in-situ gelling alginate–pectin systems and highlights their promise as gentle matrices for entrapping "bioactives" or cells[viii].

In this project, I investigate alginate–pectin blends as cell-encapsulating hydrogel fibres to function as edible, scalable scaffolds for cultivated meat. Using $CaCl_2$-mediated crosslinking and a controlled extrusion/encapsulation workflow, we explore formulation space (polymer percentages; Ca^{2+} concentration) and assess printability/handling alongside early cell outcomes (viability, morphology). The goal is to identify blend conditions that balance cell comfort (biocompatible microenvironment) with

processability (fibre integrity, handling), thereby advancing a food-grade scaffold strategy aligned with cultured-meat manufacturing constraints. Findings are discussed in the context of scaffold design rules for muscle tissue engineering and the broader sustainability and public-health motivations for alternatives to conventional livestock production[ix].

METHODOLOGY

This study investigated alginate–pectin hydrogel blends crosslinked with calcium chloride ($CaCl_2$) as potential edible scaffolds for cultivated meat applications. The methodology was designed to (i) formulate and prepare reproducible alginate–pectin solutions, (ii) implement a crosslinking strategy under sterile conditions, (iii) fabricate hydrogel fibres through both manual and device-assisted extrusion, and (iv) encapsulate C2C12 myoblasts within these scaffolds to evaluate their compatibility. Each stage of the methodology is described in detail to enable reproducibility.

Materials and Equipment

Polymers

- Sodium alginate (medium viscosity, food-grade, Sigma-Aldrich).
- Low-methoxyl pectin (degree of esterification < 50%, citrus-derived, food-grade).

Solvent

- Phosphate-buffered saline (PBS, pH 7.4, sterile-filtered).

Crosslinker

- Calcium chloride dihydrate ($CaCl_2 \cdot 2H_2O$, ≥99%, Sigma-Aldrich).

Cell Line

- C2C12 mouse myoblasts (ATCC, CRL-1772).

Consumables

- 0.22 µm PES filters.
- Sterile syringes and blunt 21–27G needles.
- 15 mL and 50 mL conical tubes.
- Sterile Petri dishes.
- 6-well tissue culture plates.

Equipment

- Magnetic stirrer with stir bars.
- Analytical balance (±0.001 g).
- Biosafety cabinet (Class II).
- Autoclave.
- pH meter.
- Fluorescence microscope.
- Büchi B-395 Pro Cell Encapsulator.

Polymer Formulation and Preparation

Alginate Stock Preparation

Sodium alginate powders were weighed and dissolved in PBS at concentrations of 1%, 2%, and 3% (w/v). Dissolution was achieved under sterile conditions by gradually sprinkling the powder into PBS while stirring continuously at room temperature. Full dissolution required 4–6 h depending on concentration. The alginate solutions were sterilised by autoclaving at 121 °C for 20 minutes. After sterilisation, they were stored at 4 °C until required.

Pectin Stock Preparation

Low-methoxyl pectin was dissolved in PBS at concentrations between 0.5% and 2% (w/v). Due to its lower solubility compared to alginate, intermittent vortexing and gentle heating (<40 °C) were applied over 6–8 h to promote dissolution. Sterilisation was performed by filtration through 0.22 µm PES filters to avoid structural degradation that may occur during autoclaving. Solutions were stored at 4 °C until use.

Blend Preparation

Blends were prepared immediately before fibre fabrication to minimise premature gelation. Alginate and pectin solutions were combined under sterile conditions in conical tubes using gentle pipette mixing to avoid bubble formation. The following formulations were tested:

- 3% alginate only (control).
- 3% alginate with 0.5% pectin.
- 3% alginate with 1% pectin.
- 3% alginate with 1.5% pectin.

Prepared blends were stored at 4 °C and used within 24 h.

Crosslinking and Fibre Formation

$CaCl_2$ Solution Preparation

$CaCl_2$ stock solutions were prepared at 1 M in PBS, sterile-filtered, and diluted to working concentrations of 50 mM, 100 mM, and 150 mM. These working solutions represented low, medium, and high crosslinking density conditions. All solutions were replaced every 48 h to maintain reproducibility.

Manual Pipette Extrusion

Hydrogel fibres were fabricated manually using sterile syringes fitted with blunt needles (21–25G). The alginate–pectin blends were loaded into syringes and extruded either dropwise or as continuous lines directly into $CaCl_2$ baths. Fibres formed instantaneously due to ionic crosslinking. The fibres were allowed to remain in the crosslinker bath for 5 min to ensure complete gelation. After crosslinking, fibres were rinsed twice in PBS to remove unbound calcium ions and stored in sterile PBS until use.

Device-Assisted Fabrication with Büchi B-395 Pro

To improve uniformity, hydrogel fibres were also fabricated using the Büchi B-395 Pro Cell Encapsulator. The device was sterilised before use by flushing with 70% ethanol followed by sterile PBS. A sterile nozzle assembly (e.g. 150 µm diameter) was fitted to the system. Device parameters were adjusted to enable continuous fibre production:

- Flow rate: 2–5 mL/min.
- Vibration frequency: 1000–1500 Hz.
- Voltage: 800–1200 V (for electrostatic dispersion where applied).

- Distance from nozzle to $CaCl_2$ bath: 2–4 cm.

Polymer solutions were extruded into $CaCl_2$ baths under these conditions and fibres were allowed to crosslink for 5 min. Crosslinked fibres were washed twice in PBS and collected in sterile Petri dishes.

Scaffold Characterisation

Fibre Morphology

Digital images of fibres were captured through the biosafety cabinet. Diameters were measured using ImageJ at ten random points per fibre. Manual and encapsulator-derived fibres were compared for uniformity and reproducibility.

Mechanical Handling

Fibres were assessed qualitatively for robustness during handling with sterile forceps. Samples were classified as robust (intact and bendable), moderate (deformed but intact), or weak (fragmented). Scores were averaged across three replicates for each condition.

Swelling and Stability

Fibres were incubated in PBS at 37 °C for 1 h, 24 h, and 72 h. Dimensional changes and structural integrity were recorded. Stability was categorised as stable, partially degraded, or fully degraded.

Sterility Checks

Sterility was verified by inoculating 1 mL aliquots of polymer solutions into LB broth, followed by incubation at 37 °C for 48 h. Samples with no turbidity were considered sterile. In addition, no-cell fibres were incubated in culture media alongside cell-laden fibres to confirm the absence of microbial contamination from polymer batches.

Cell Encapsulation and Culture

Cell Preparation

C2C12 myoblasts were cultured in Dulbecco's Modified Eagle Medium (DMEM) supplemented with 10% foetal bovine serum and 1% penicillin–streptomycin. Cultures were maintained at 37 °C in a 5% CO_2 humidified incubator. Cells were expanded to 70–80% confluency, detached using 0.05% trypsin–EDTA, centrifuged at 300 g for 5 min, and resuspended in fresh culture medium. Cell suspensions were adjusted to [insert final density used, e.g. 2×10^6 cells/mL].

Manual Encapsulation

Cell suspensions were gently mixed into alginate–pectin blends under sterile conditions. The resulting mixtures were loaded into sterile syringes and extruded into $CaCl_2$ baths at concentrations of 50–150 mM. Encapsulation occurred immediately upon fibre formation. After 5 min, fibres were rinsed twice with PBS and transferred into 6-well plates containing pre-warmed culture medium.

Encapsulation with Büchi B-395 Pro

For device-assisted encapsulation, alginate–pectin blends containing C2C12 cells were loaded into the encapsulator reservoir. Parameters were adjusted to reduce shear stress while maintaining uniform fibre production. The same nozzle size and flow ranges used for polymer-only experiments were applied. Fibres were collected in $CaCl_2$ baths, crosslinked for 5 min, rinsed with PBS, and transferred into 6-well plates with culture medium.

Post-Encapsulation Culture

Cell-laden fibres were incubated at 37 °C, 5% CO_2. Culture medium was replaced every 48 h for up to 7 days, then cells transferred to differentiation media. Samples were collected at 24 h, 48 h, and 72 h to assess viability and morphology.

Viability and Morphology Assays

Fibres were incubated with live/dead fluorescent dyes (calcein AM for live cells and propidium iodide for dead cells). Imaging was performed with a fluorescence microscope and viability was calculated as the percentage of live cells across five random fields of view. In addition, fibres were examined under bright-field microscopy to evaluate cell morphology, including roundness, elongation, and alignment along the fibre axis. For cell counting, enzymatic digestion with alginate lyase and pectinase was used to release encapsulated cells, which were then counted with a haemocytometer.

Replicates and Statistical Analysis

All formulations and conditions were tested in triplicate across at least three independent experimental runs. Data were expressed as mean ± standard deviation. Statistical significance was evaluated using one-way ANOVA followed by Tukey's post hoc test in GraphPad Prism. Significance was defined at $p < 0.05$.

Parameter	Levels used	Notes
Alginate	1, 2, 3% w/v	Medium-viscosity SA
Pectin	0–1.5% w/v	Low-methoxyl (DE <50%)
$CaCl_2$ bath	50, 100, 150 mM; **3% w/v** in Fig. X	Specify molarity in captions
Nozzle	200–300 µm	State per figure
Vibration	0–5000 Hz	Device % as used
Flow	0.9–1.5 "L" (your unit)	Replace with **mL/min** for clarity
Cells	C2C12, 3×10^6 cells/mL	Passage range
Dyes	Calcein AM / EthD-1 (or PI)	Concentrations, incubation time

Methodology Summary

In summary, this methodology combined alginate–pectin blend formulation, ionic crosslinking in $CaCl_2$ baths, manual and device-assisted fibre fabrication, and encapsulation of C2C12 myoblasts. Fibres were characterised for morphology, diameter uniformity, mechanical handling, swelling behaviour, stability, and sterility. Encapsulated cells were analysed for viability, morphology, and proliferation over 72 h. This workflow provides a reproducible strategy for evaluating alginate–pectin blends as candidate scaffolds for cultivated meat production.

RESULTS AND DISCUSSION

We investigated the effect of alginate concentration and collection geometry on fibre formation and myoblast response. Sodium alginate solutions at 1–3% (w/v) were extruded into $CaCl_2$ baths using either a benchtop encapsulator or manual pipetting. Morphology, handling, and thermal stability were assessed, then C2C12 cells were encapsulated and cultured to Day 9 with live/dead imaging. Results are presented by concentration, followed by alignment and cell outcomes.

Mean fibre diameter increased with alginate concentration (1%: 128 ± 46 µm, 2%: 212 ± 58 µm, 3%: 301 ± 41 µm; n=30 per group). Coefficient of variation fell from 36% (1%) to 14% (3%). Live cell fraction at D3 was higher in manual fibres than encapsulator aggregates or large droplets (0.78 ± 0.06 vs 0.61 ± 0.08 and 0.34 ± 0.09, respectively; p<0.01). At D9, elongated cells were most frequent on anisotropic filaments (encapsulator), whereas manual fibres retained mostly rounded morphologies despite high viability (qualitative scoring; propose adding orientation index).

To evaluate the effect of alginate concentration on fibre formation, fibres were produced at 1%, 2%, and 3% (w/v) sodium alginate using the Büchi B-395 Pro Cell Encapsulator. Each concentration was examined under multiple vibration frequencies and flow rates to determine the conditions that supported stable fibre formation. Representative fibres were imaged at both 4× and 10× magnification and assessed qualitatively for structural integrity, morphology, and handling robustness. Results are presented in ascending order of concentration, beginning with 1% alginate fibres, which serve as the lower-concentration control, followed by 2% and 3% alginate fibres.

1% alginate fibres

Fibres produced from 1% (w/v) alginate consistently displayed poor structural integrity across all encapsulator settings. At 0 Hz vibration (0Hz 30% 1L 4x 2, 0Hz 30% 1L 4x 3), the material formed folded mats and collapsed sheets rather than continuous cylindrical strands. Higher magnification images (0Hz 30% 1L 10x, 0Hz 30% 1L 10x) revealed corrugated surfaces with local nodes and necking, indicating instability during jet breakup. These morphologies are consistent with insufficient chain entanglement at low alginate concentration and the formation of a thin crosslinked shell that subsequently buckled during external gelation.

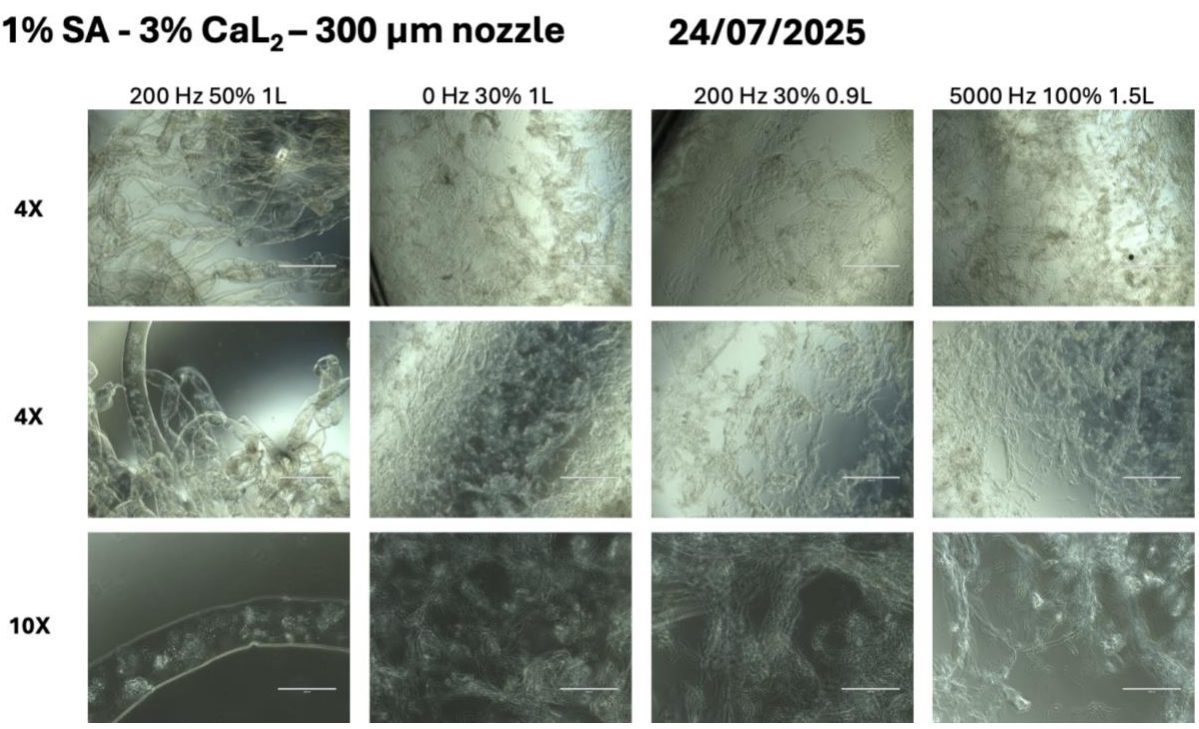

At 200 Hz without additional amplitude adjustment (200Hz 0% 1L 4x 1, 200Hz 0% 1L 4x 2), fibres were fragmented into short, tangled segments with little continuity. At higher magnification (200Hz 0% 1L 10x 4), overlapping folds and tearing were apparent. Increasing the amplitude to 30% while slightly reducing flow (200Hz 30% 0.9L 4x, 200Hz 30% 0.9L 4x 5) marginally improved edge definition, but the fibres remained curled and discontinuous, with higher magnification views (200Hz 30% 0.9L 10x 7) confirming wrinkled skins and scalloped edges.

At 200 Hz with 50% amplitude (200Hz 50% 1L 4x 6.tif, 200Hz 50% 1L 4x.tif, 200Hz 50% 1L.tif), some evidence of more continuous strands was observed. However, fibres were typically ribbon-like, brittle, and uneven in width, with abrupt thinning and thickened nodes. Images at higher magnification (200Hz 50% 1L 10x 7, 200Hz 50% 1L 10x 8.tif, 200Hz 50% 1L 10x 9) revealed porous, collapsed surfaces with a rough texture, suggesting rapid water loss during Ca^{2+} diffusion and incomplete core gelation.

At very high frequency and amplitude (5000Hz 100% 1.5L 4x 1, 5000Hz 100% 1.5L 4x 2), fibres fragmented almost immediately into short bead-like segments and irregular clumps, with no continuous structure. Higher magnification images (5000Hz 100% 1.5L 10x 2, 5000Hz 100% 1.5L 10x 3) confirmed bead-on-a-string morphologies and collapsed fragments. This behaviour is characteristic of Rayleigh–Plateau instability under strong perturbation when the polymer concentration is insufficient to sustain filamentary flow.

Taken together, fibres formed from 1% alginate were consistently shrivelled, sheet-like, or fragmented, irrespective of vibration frequency or flow conditions. This outcome can be attributed to the polymer concentration being below the overlap threshold required for stable chain entanglement, leading to poor viscoelastic resistance against jet breakup. Rapid surface crosslinking by Ca^{2+} ions further accentuated collapse by producing a fragile skin around an unstructured core. Consequently, 1% alginate could not produce fibres with the structural robustness required for scaffold applications.

2% alginate fibres

Fibres fabricated from 2% (w/v) alginate showed markedly improved structural definition compared to 1% samples. At 0 Hz, 0% amplitude, and 0.9 L flow, fibres exhibited partial continuity but remained irregular, with overlapping sheets and ribbon-like morphologies visible at 2× and 4× magnification. Higher

magnification (10×) revealed flattened fibres with variable thickness and local folding. Although cohesion was superior to 1% alginate, the fibres were still prone to collapse during collection, reflecting insufficient viscoelasticity at this concentration to maintain cylindrical geometry without vibration.

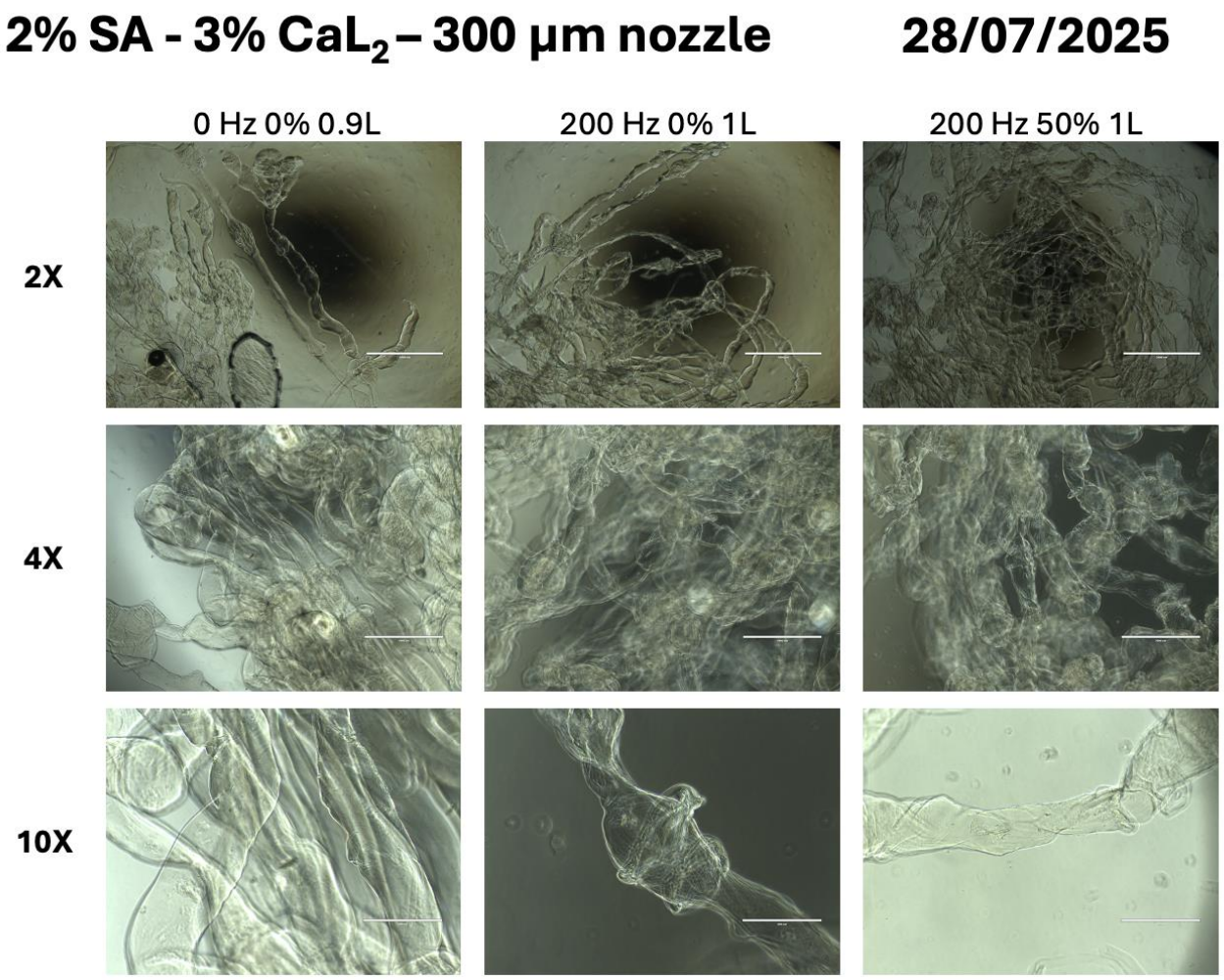

At 200 Hz with 0% amplitude and 1 L flow, fibres were more uniform and continuous. Low-magnification images showed networks of interconnected strands, and higher magnification demonstrated smoother surfaces relative to the 0 Hz condition. However, occasional necking and irregular diameters persisted, indicating that while vibration stabilised the jet, crosslinking remained heterogeneous.

At 200 Hz with 50% amplitude and 1 L flow, fibres displayed the most consistent morphology. Bundles appeared thicker and more resilient, with reduced folding and fewer collapsed sheets compared to other conditions. At 10× magnification, fibres maintained cylindrical form but showed periodic constrictions, producing a bead-on-a-string appearance. This morphology suggests that vibration at higher amplitude improved filament stability during extrusion but that 2% alginate still lacked sufficient chain overlap to fully suppress capillary instabilities.

Overall, 2% alginate fibres represented a clear improvement over 1%, producing continuous strands under multiple settings, particularly at intermediate vibration. However, fibres remained fragile, prone to local collapse, and lacked the robustness expected for scaffold applications. This behaviour reflects the transition region where alginate concentration begins to approach but does not consistently exceed the overlap threshold necessary for stable filament formation.

3% alginate fibres

Fibres fabricated from 3% (w/v) alginate demonstrated the most consistent morphology and structural integrity of all concentrations tested. At 0 Hz, 10% amplitude, and 1 L flow, fibres were continuous and well-defined, forming bundles visible at low magnification (2×). At 4× magnification, fibres retained cylindrical geometry with minimal collapse and smoother surfaces compared to 1% and 2% samples. At 10× magnification, fibres displayed uniform diameters and intact cores, indicating that increased alginate concentration provided sufficient chain entanglement to suppress jet breakup and resist buckling during external crosslinking.

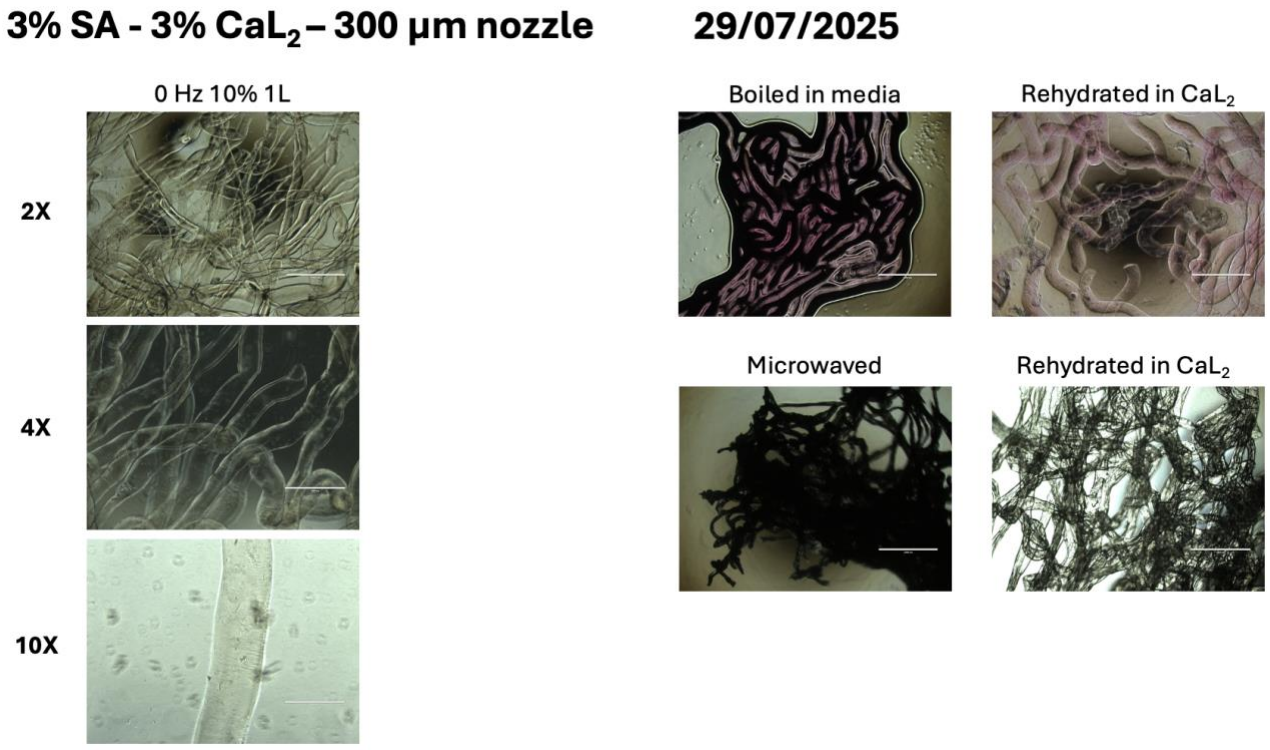

To evaluate thermal and rehydration stability, fibres were subjected to boiling in culture medium, microwave heating, and subsequent rehydration in $CaCl_2$ solution. Fibres boiled in medium collapsed into dense, ribbon-like structures, while microwaved fibres formed compact, aggregated clumps, both consistent with thermal destabilisation of ionic crosslinks. By contrast, rehydration in $CaCl_2$ partially restored fibre continuity, with networks of interconnected strands visible at both conditions tested. These observations suggest that although thermal treatment disrupts the Ca^{2+}–alginate junctions, exposure to fresh Ca^{2+} can re-establish crosslinking, underscoring the reversible ionic nature of the network.

Overall, 3% alginate fibres exhibited robust morphology during fabrication and greater resilience to processing than fibres at lower concentrations. However, their sensitivity to heating highlights the need for careful consideration of downstream processing and storage conditions in potential scaffold applications.

A clear concentration-dependent effect was observed across the three alginate formulations. Fibres produced at 1% alginate consistently lacked continuity, forming collapsed sheets or fragmented droplets regardless of encapsulator parameters. At 2%, fibres demonstrated partial improvements, with more continuous strands under certain vibration settings, although collapse and irregular morphologies

persisted. In contrast, 3% alginate yielded robust, cylindrical fibres with minimal collapse, confirming that higher polymer concentration provides the necessary chain overlap and viscoelasticity to stabilise jet formation and resist crosslinking-induced buckling. These results establish 3% alginate as the most suitable baseline concentration for scaffold fabrication under the tested conditions.

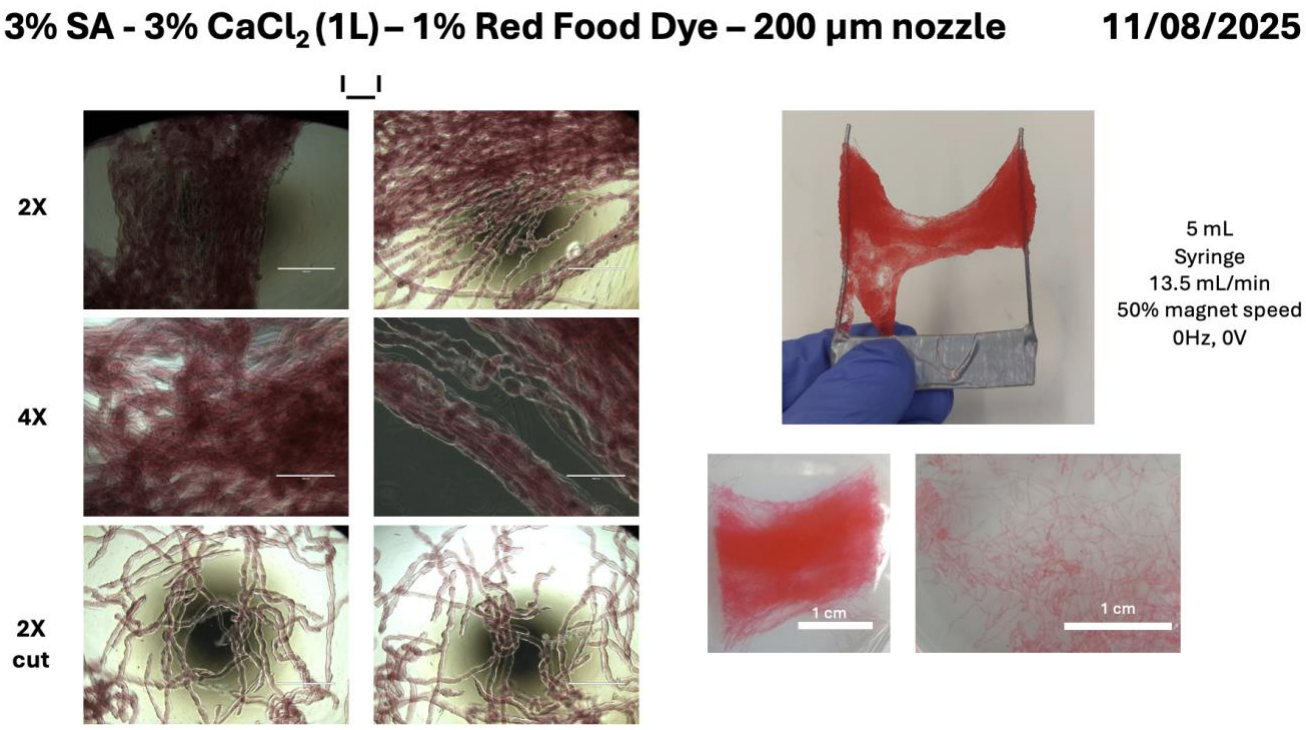

Fibre alignment and collection

To enhance structural organisation, a custom attachment was fabricated for the magnetic stirrer consisting of two parallel stainless-steel wires that enabled fibres to be collected in an aligned manner during extrusion. Alignment is a key design parameter for muscle tissue engineering, as myoblasts require anisotropic physical cues to elongate, align, and subsequently fuse into multinucleated myotubes. Randomly oriented scaffolds fail to provide this guidance, leading to heterogeneous differentiation and limited contractile function, whereas aligned scaffolds mimic the native extracellular matrix of skeletal muscle and promote ordered sarcomere formation. Introducing mechanical anisotropy into hydrogel fibres is therefore critical for their use as cultivated-meat scaffolds, where aligned fibres can help recapitulate the texture and structural integrity of conventional muscle.

Morphological assessment of aligned fibres

The addition of red food dye allowed improved visualisation of fibres under both optical microscopy and macroscopic imaging. At low magnification (2×), fibres collected on the wire frame formed extended bundles spanning the collection area, showing clear directional alignment relative to uncollected conditions. At higher magnification (4×), fibres appeared as densely packed sheets with parallel orientation and reduced folding compared to earlier unaligned preparations. At 10× magnification, individual fibres retained cylindrical morphology with uniform staining, suggesting consistent dye incorporation without disrupting crosslinking.

The macroscopic images confirm the efficacy of the alignment strategy. Fibres were suspended across the wire frame in a planar sheet, which could be handled and manipulated without disintegration. Once dried,

the aligned constructs retained their orientation, although local compaction was observed. Cut sections imaged at 2× revealed regular parallel arrays, while separate images of detached fibre mats demonstrate that the red dye diffused homogeneously throughout the network.

Structural robustness and handling

Aligned fibre mats displayed sufficient cohesion to be lifted from the collection bath and manipulated manually, as shown in the photographs of the scaffold held by gloved hands. This represents a marked improvement in scalability and practical handling relative to previous unaligned fibres, which were fragile and prone to collapse. The cut 2× images further highlight how the alignment collector reduced fibre entanglement, producing more defined bundles suitable for downstream testing.

Implications

These results demonstrate that simple modifications to the collection system can transform the structural organisation of alginate fibres, yielding aligned constructs with greater handling robustness. The ability to generate aligned hydrogel scaffolds is directly relevant for skeletal muscle engineering, where cell orientation is essential for differentiation and maturation. The successful incorporation of food dye also illustrates how visual tracking of fibres can aid in both experimental optimisation and potential industrial workflows.

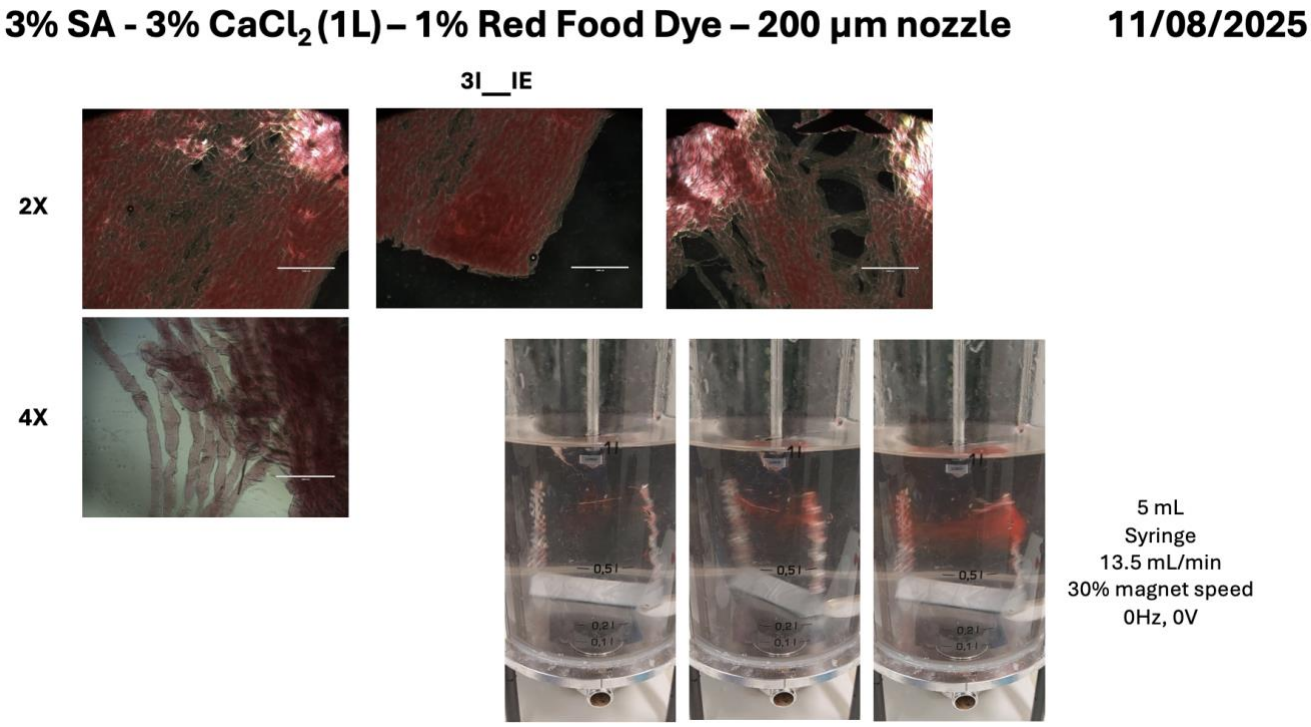

Macroscopic assembly of aligned fibre mats

To further evaluate the scalability of the alignment approach, fibres were extruded into a wire collector submerged in a stirred $CaCl_2$ bath and subsequently stained with red food dye for improved contrast. At low magnification (2×), fibres deposited on the collector formed thick, sheet-like mats with densely interwoven filaments, in contrast to the looser bundles observed in earlier unaligned experiments. Higher magnification (4×) revealed distinct, parallel fibre tracks with minimal folding, indicating that the alignment system not only facilitated directional organisation but also reduced fibre entanglement during crosslinking. Surface imaging of the dried mats (2× top panels) showed a cohesive structure with local compaction and interconnected pores, suggesting that aligned collection also enhances fibre-to-fibre junctions that contribute to bulk stability.

Macroscopic views of the collection process in the stirred bath (bottom row) further illustrate the progressive build-up of fibre mats between the wire supports. The construct maintained tension across the collector frame as additional fibres were deposited, yielding a planar sheet that could be manipulated without disintegration. The red staining highlights the accumulation of multiple fibre layers over time, producing a scaffold with millimetre-scale dimensions. These images collectively demonstrate that aligned fibre deposition can be scaled to generate macroscopically robust mats rather than isolated microfibres.

Implications for scaffold engineering

The ability to assemble continuous sheets of aligned fibres represents a significant step toward functional muscle-mimetic scaffolds. Aligned fibre mats can provide anisotropic mechanical properties and topographical cues that guide myoblast elongation and fusion, while the emergent bulk structure offers improved handling for downstream culture and potential integration into bioreactor systems. The observation that fibres remain cohesive under magnetic stirring conditions further underscores their suitability for scaled-up fabrication workflows. Together, these results demonstrate how combining controlled fibre extrusion with guided collection enables the transition from fragile microstructures to mechanically resilient, macroscopically organised scaffolds.

Integration of alignment with stability considerations

The macroscopic fibre mats produced with the alignment collector complement the earlier thermal stability studies. Whereas fibres boiled or microwaved exhibited severe collapse due to disruption of ionic Ca^{2+} crosslinks, the aligned mats retained cohesion even under continuous stirring during fabrication. This contrast highlights that scaffold robustness is influenced not only by polymer concentration and crosslinking chemistry but also by the way fibres are assembled. Aligned collection promotes inter-fibre contacts and mechanical reinforcement within the scaffold, which may buffer against stresses that would otherwise lead to fragmentation in isolated fibres. Rehydration experiments further demonstrated that ionic junctions can be re-established following disruption, suggesting that aligned mats could similarly recover structural integrity if destabilised. Together, these findings indicate that achieving both alignment and bulk connectivity is essential for scaffolds intended to withstand processing and culture conditions while maintaining the anisotropic cues necessary for myogenic differentiation.

Live/dead assessment of encapsulated C2C12 cells

Day 0 (seeding)

At the time of encapsulation, cells were introduced into alginate–$CaCl_2$ blends using either the Büchi encapsulator or manual pipetting. Encapsulator attempts yielded no continuous fibres and instead produced blobs with sheared fragments, despite correct nozzle calibration and sterilisation. In contrast, manual extrusion with 10 µL pipette tips generated continuous fibres containing uniformly distributed cells, with no obvious fibre damage and encapsulation efficiency estimated at ~30,000 cells per fibre. These results established manual pipetting as a reproducible baseline method for ensuring initial encapsulation.

Differentiation Experiment 1 08.09.25

- **D0** Seeding 3x10^6 cells/mL in **Growth** Media

Encapsulator:

- didn't work, no fibres, blob formations with sheared fibres
- 120 µL nozzle, no obstruction
- 8 mL/min, 40% magnet speed
- All parts sterilised separately

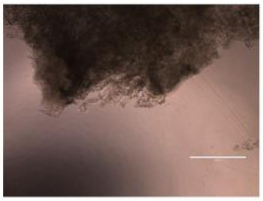
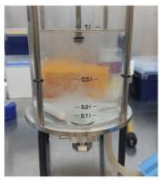
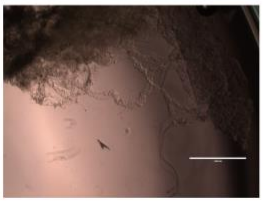
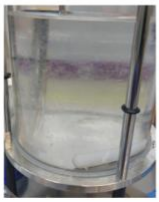

Manual:

- 10 µL tips, pipetted vertically in 20 mL $CaCl_2$ cs

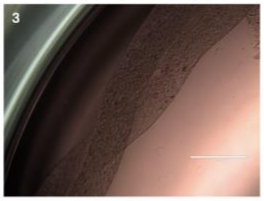

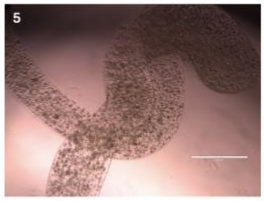

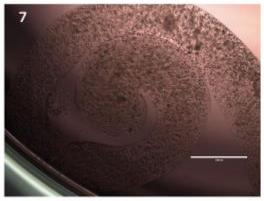

- Cells successfully encapsulated
- No fibre damage
- All fibres are 10 µL → 30000 cells

Day 3 (switch to differentiation medium)

Live/dead staining at Day 3 revealed stark differences across conditions. Encapsulator-derived aggregates contained both viable (green) and non-viable (red) cells, with pockets of elongating cells visible at the periphery. The majority of encapsulated cells in this group were rounded, suggesting limited early adhesion and alignment but with evidence of partial survival. Manual 10 µL fibres showed high viability overall, with predominantly green-stained cells; however, the cells remained largely spherical, with no consistent elongation observed at this stage. In contrast, 200 µL bulk droplets exhibited poor viability, with extensive red staining indicative of necrosis. The large constructs likely developed hypoxic or nutrient-limited cores, consistent with necrotic centre formation, and viability gradients were visible from edge to centre.

Together, Day 3 data indicate that smaller manual fibres support more uniform viability compared to encapsulator-derived aggregates or large droplets. The occasional elongation in encapsulator samples may reflect localised cell–cell contact and differentiation signals, though overall structure was compromised.

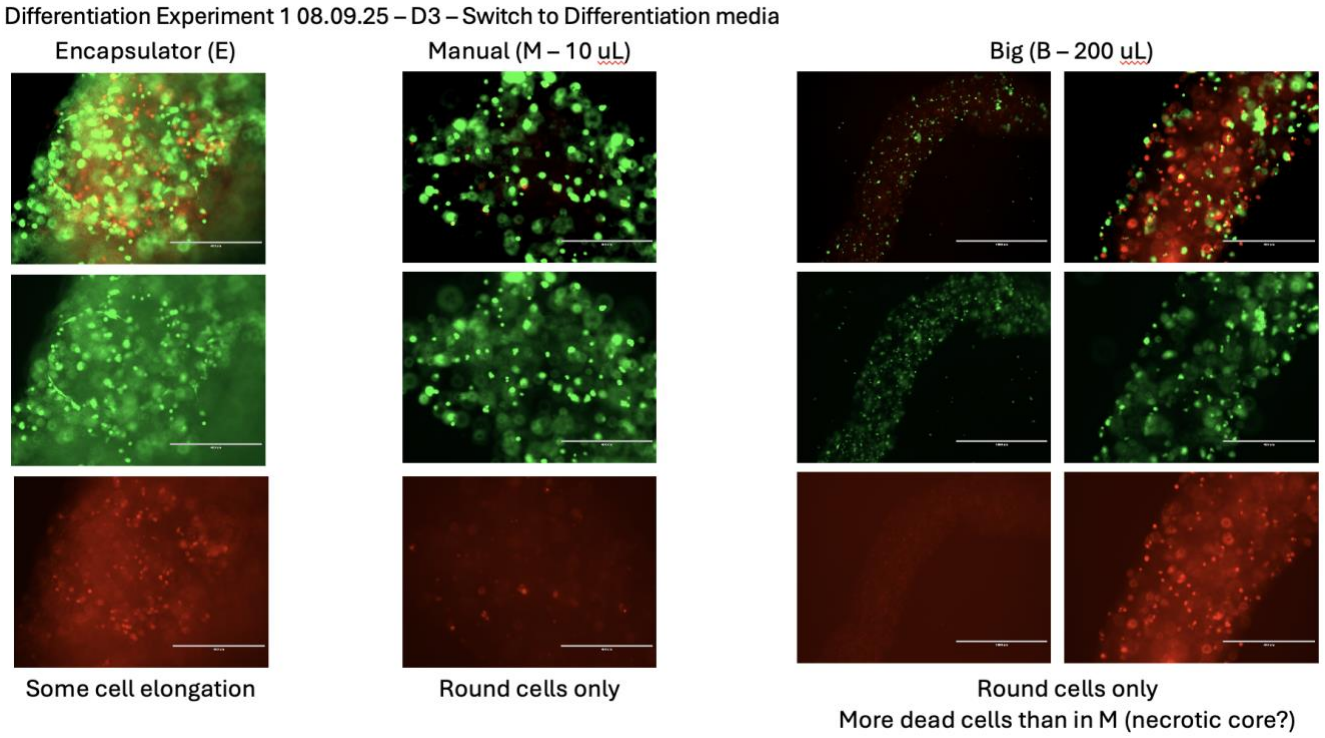

Day 6

By Day 6, differences between conditions were further pronounced. Encapsulator-derived fibres exhibited visible elongation of C2C12 cells along thin strands, with green-stained cells aligning preferentially along fibre tracks. This suggests that, despite initial inefficiencies in fibre production, the small, irregular filaments that did form provided sufficient topographical cues to promote early elongation. Manual fibres retained high viability but remained dominated by round morphologies, suggesting that while encapsulation and nutrient diffusion were sufficient to maintain survival, the scaffold geometry was not consistently triggering alignment. In the 200 µL droplets, structural integrity deteriorated significantly; fibres were weak and often dissolved, releasing cells into the medium. Cells displayed poor viability overall, with scattered red-stained populations indicating widespread necrosis. These findings reinforce the importance of scaffold microarchitecture in directing cell fate: thin encapsulator-derived filaments, despite their fragility, were able to trigger alignment responses not seen in bulk manual or large droplet formats.

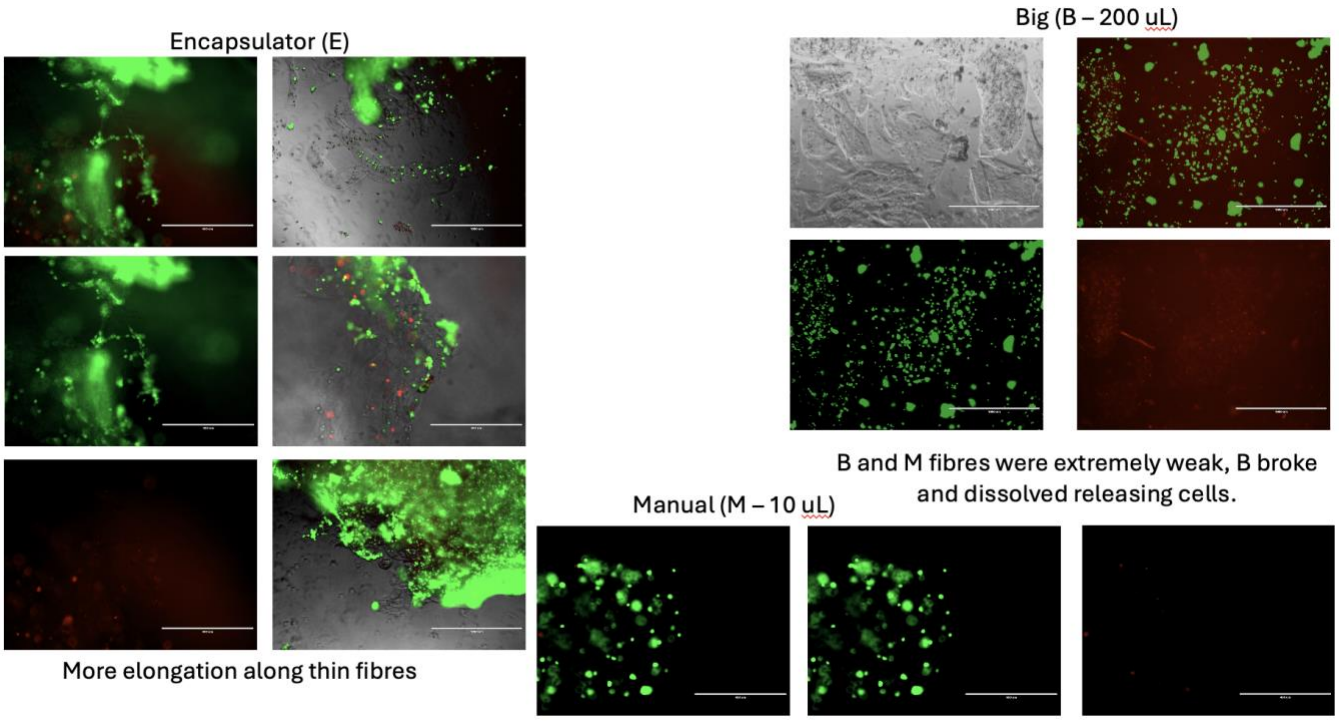

Day 9

At Day 9, encapsulator-derived filaments demonstrated the clearest signs of differentiation. Green-stained cells displayed elongated morphologies aligned with fibre direction, forming early myotube-like structures. Red-stained populations were present but remained localised, suggesting partial but not complete scaffold support. Manual 10 µL fibres sustained high viability with relatively few dead cells, yet the majority of cells remained spherical, highlighting a limitation in their capacity to drive myogenic differentiation under the tested conditions. The 200 µL droplets continued to exhibit poor outcomes: extensive red staining dominated the constructs, with many cells appearing necrotic, consistent with collapse of scaffold structure and inadequate nutrient delivery.

Differentiation Experiment 1 08.09.25 – D9

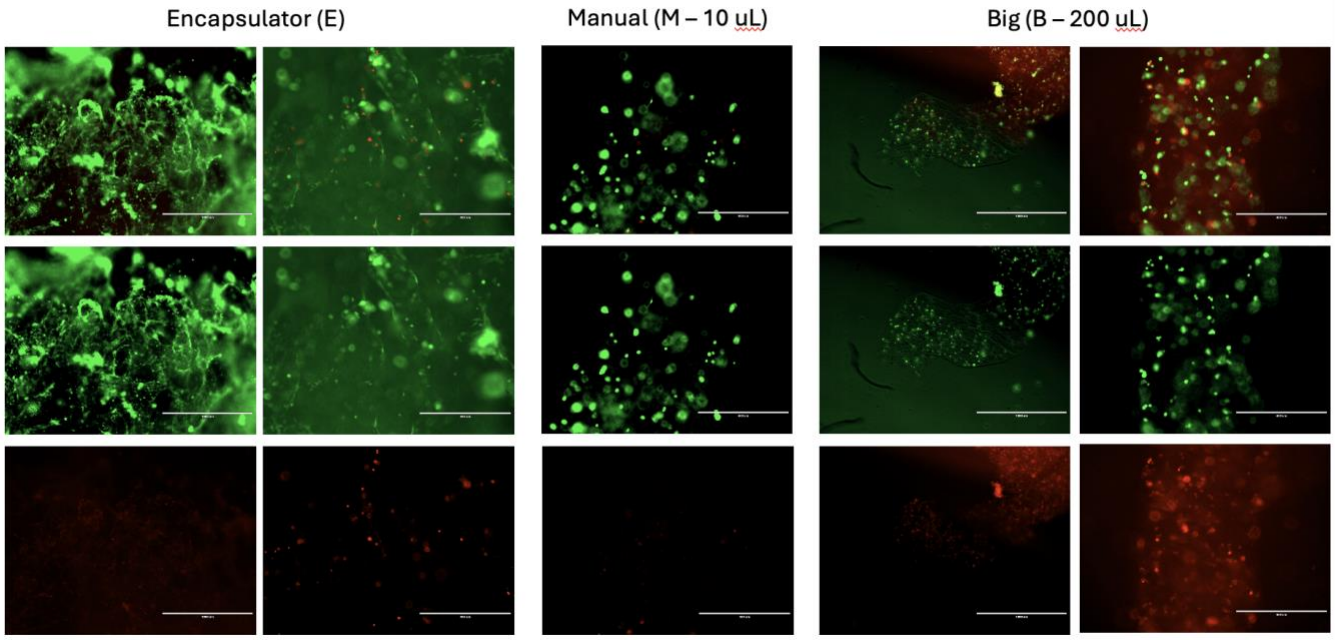

Elongation around fibres

Comparative insights

1. **Encapsulation format dictates viability and morphology.**
    - Manual 10 µL fibres offered reliable survival but lacked directional cues.
    - Encapsulator-derived filaments, though inconsistent in formation, promoted elongation and alignment, demonstrating the critical role of anisotropy in guiding myogenesis.
    - Large 200 µL droplets were structurally unstable and developed necrotic cores, making them unsuitable for long-term culture.
2. **Fibre geometry influences differentiation.**
    - Alignment observed in encapsulator samples underscores the importance of topographical guidance, echoing prior scaffold literature where aligned microstructures accelerate myoblast fusion.
    - Manual fibres, though robust, may require secondary alignment strategies (e.g. collector systems or mechanical tensioning) to induce differentiation.
3. **Time-dependent outcomes.**
    - Early survival (Day 3) was highest in manual fibres.
    - Differentiation cues (Day 6–9 elongation) were more evident in encapsulator filaments, albeit with structural fragility.
    - Large droplets progressively failed, collapsing by Day 6 and necrotic by Day 9.

Overall interpretation

Live/dead assays demonstrated that **manual extrusion reliably produces cell-laden fibres with high viability**, while **encapsulator-derived filaments, despite technical difficulties, may better support elongation and differentiation** due to anisotropic fibre morphology. By contrast, **large droplets are unsuitable**, as they consistently failed to maintain structural integrity or cell viability. These findings emphasise the dual importance of **viability (ensured by fibre scale)** and **anisotropy (driven by alignment and scaffold geometry)** in engineered muscle constructs.

CONCLUSION

This study set out to fine tune alginate–pectin hydrogel scaffolds as edible, scalable supports for cultivated meat production. Across concentration screening, alignment optimisation, and cell encapsulation experiments, several key principles for scaffold design emerged.

First, fibre morphology was highly concentration dependent. At 1% alginate, fibres consistently collapsed into sheets or fragmented beads, reflecting insufficient chain entanglement to resist crosslinking stresses. Increasing to 2% improved continuity under certain vibration settings, but fibres remained fragile and prone to collapse. By contrast, 3% alginate yielded the most robust, cylindrical fibres with smooth surfaces and consistent handling properties. These concentration effects highlight the importance of achieving polymer overlap thresholds for stable filament formation and establish 3% alginate as a practical baseline for scaffold fabrication.

Second, scaffold organisation was shown to be as critical as polymer concentration. Modifications to the collection system, using wire supports to align fibres during extrusion, transformed randomly entangled mats into highly ordered bundles and sheet-like assemblies. Aligned fibres not only improved mechanical handling but also introduced the anisotropic architecture known to be essential for myoblast elongation, alignment, and eventual fusion into myotubes. These results underline that bulk organisation and anisotropy must be incorporated into scaffold design if muscle-mimetic texture and function are to be achieved.

Third, functional stability of the scaffolds was demonstrated to be sensitive to processing. Thermal treatments such as boiling or microwaving disrupted ionic crosslinks, leading to fibre collapse, whereas rehydration in calcium chloride partially restored network integrity. This reversible behaviour reflects the ionic nature of Ca^{2+}–alginate junctions and points to both a challenge and opportunity: while thermal processing can compromise fibre structure, controlled re-crosslinking offers a route for recovery.

Finally, cell encapsulation experiments revealed how scaffold geometry dictates cell fate. Manual extrusion of 10 µL fibres consistently supported high viability, though cells remained largely spherical over time, suggesting limited differentiation cues. Encapsulator-derived filaments, although technically inconsistent, produced anisotropic fibre geometries that promoted visible elongation and alignment of C2C12 cells by Day 6–9, resembling early myotube formation. Large 200 µL droplets performed poorest, showing rapid necrosis due to hypoxic cores and loss of structural integrity. Together, these findings establish that both scaffold **scale** and **anisotropy** must be optimised to balance survival and differentiation.

In sum, this work demonstrates that **3% alginate fibres, collected in aligned configurations, represent a promising edible scaffold system for cultivated meat applications**. While manual extrusion offers robust survival, alignment strategies are necessary to drive myogenic differentiation. Encapsulator-based fabrication remains attractive for producing anisotropic filaments but requires further optimisation to achieve reproducibility. The study reinforces that cultivated meat scaffold design cannot rely on single parameters such as concentration alone, but must integrate polymer physics, alignment, stability, and cell–material interactions into a coherent strategy.

Future work should explore blend formulations (e.g. alginate–pectin mixtures) to further modulate gelation kinetics and mechanical properties, and test bioreactor-based alignment strategies to achieve macroscale muscle tissue. By advancing scaffold systems that combine food-grade chemistry, processability, and

biological functionality, these findings contribute to the engineering principles needed to realise structured, sustainable cultivated meat.

REFERENCES

[i] Poore, J. and Nemecek, T. (2018). Reducing Food's Environmental Impacts through Producers and Consumers. Science, 360(6392), pp.987–992. doi:https://doi.org/10.1126/science.aaq0216.

[ii] Broom, D.M. (2010). Animal Welfare: An Aspect of Care, Sustainability, and Food Quality Required by the Public. Journal of Veterinary Medical Education, 37(1), pp.83–88. doi:https://doi.org/10.3138/jvme.37.1.83.

[iii] Van Boeckel, T.P., Brower, C., Gilbert, M., Grenfell, B.T., Levin, S.A., Robinson, T.P., Teillant, A. and Laxminarayan, R. (2015). Global trends in antimicrobial use in food animals. Proceedings of the National Academy of Sciences, 112(18), pp.5649–5654. doi:https://doi.org/10.1073/pnas.1503141112.

[iv] Marshall, B.M. and Levy, S.B. (2011). Food Animals and Antimicrobials: Impacts on Human Health. Clinical Microbiology Reviews, [online] 24(4), pp.718–733. doi:https://doi.org/10.1128/cmr.00002-11.

[v] Tuomisto, H.L. and Teixeira de Mattos, M.J. (2011). Environmental Impacts of Cultured Meat Production. Environmental Science & Technology, [online] 45(14), pp.6117–6123. doi:https://doi.org/10.1021/es200130u.

[vi] Ben-Arye, T. and Levenberg, S. (2019). Tissue Engineering for Clean Meat Production. Frontiers in Sustainable Food Systems, [online] 3. doi:https://doi.org/10.3389/fsufs.2019.00046.

[vii] Cao, L., Lu, W., Mata, A., Nishinari, K. and Fang, Y. (2020). Egg-box model-based gelation of alginate and pectin: A review. Carbohydrate Polymers, 242, p.116389. doi:https://doi.org/10.1016/j.carbpol.2020.116389.

[viii] Del Gaudio, P., Amante, C., Civale, R., Bizzarro, V., Petrella, A., Pepe, G., Campiglia, P., Russo, P. and Aquino, R.P. (2020). In situ gelling alginate-pectin blend particles loaded with Ac2-26: A new weapon to improve wound care armamentarium. Carbohydrate Polymers, 227, p.115305. doi:https://doi.org/10.1016/j.carbpol.2019.115305.

[ix] A.M.M. Nurul Alam, Kim, C.-J., Kim, S.-H., Kumari, S., Lee, E.-Y., Hwang, Y.-H. and Joo, S.-T. (2024). Scaffolding fundamentals and recent advances in sustainable scaffolding techniques for cultured meat development. Food Research International, 189, pp.114549–114549. doi:https://doi.org/10.1016/j.foodres.2024.114549.